Universitat de les Illes Balears

Potential vorticity error assessment applied to ensemble forecasts of Mediterranean cyclones

By
Maria del Mar Vich Ramis

Final Thesis of Masters in Physics
September, 2007

Director: Dr. Romualdo Romero March

Contents

Abstract

The western Mediterranean is a very cyclogenetic area and many of the cyclones developed over that region are associated with high impact weather phenomena that affect the society of the coastal countries. In order to improve the short and mid-range numerical forecasts of cyclones, ensemble prediction systems based on perturbed initial and boundary conditions are being designed. A potential vorticity inversion technique is used to perturb the initial state and boundary forcing of a mesoscale model. These simulations are performed with the MM5 mesoscale model nested in the ECMWF forecast large-scale fields, which provides results at 22.5 km resolution for a two-day period over the western Mediterranean countries.

In an attempt to introduce realistic perturbations in the ensemble prediction system, a PV error climatology (PVEC) is derived. This climatology allows to perturb the ECMWF forecast PV fields using the appropriated error range. The PVEC is calculated using a large collection of MEDEX cyclones, and provides the displacement and intensity error of the PV fields in the study region. Analytical functions have been fitted to model the error statistics (percentile levels of displacement and intensity errors) as function of pressure level and PV value. This PVEC is used to implement the above mentioned ensemble system by randomly perturbing the fields. Preliminary results show precipitation fields of realistic variability.

Chapter 1

Introduction

The Mediterranean climate is characterized by moist mild winter and dry hot summer. A notorious characteristic of this climate is an autumn season with torrential rainfall following a drought period of various months. These heavy rain events have a high impact in the society due to floods and economical losses. So, a primary objective in the Mediterranean region is to improve the prediction of these events to prevent or reduce the damages.

Figure 1.1. *The western Mediterranean area*

The western Mediterranean (Fig. 1.1) is a very cyclogenetic area and several studies have established a connection between heavy rainfall and cyclones over this region (Jansà et al., 2001). A good knowledge of the Mediterranean cyclogenesis[1] related to rain systems is thus needed.

[1]Cyclogenesis: birth and development of a cyclone

Some examples of cyclones associated to heavy rain events are:

– shallow weak disturbances with a warm core over land masses of thermal origin (Romero et al., 2001),

– shallow weak lows with a warm core over the sea at the lee of important mountain ranges, linked to the orographic effect on the atmospheric flow (Romero et al., 2000), and

– baroclinic systems with great vertical amplitude (Homar et al., 2002), developed along frontal zones under the intrusion in the Mediterranean region of an upper-level through.

In addition to understanding the Mediterranean cyclogenesis, a prediction system with good performance is also needed. In order to achieve this goal, a dynamical and statistical technique based on numerical simulations and post-processed forecast fields (probabilistic strategy) is applied in this master thesis. In other regions of the world, probabilistic forecasting systems have been successfully applied with even better detection skill of extreme events than the traditional deterministic forecasting.

The probabilistic forecasting is applied through an ensemble prediction system based on perturbed initial and boundary conditions. The numerical simulations are performed with the MM5 mesoscale model and the used data comes from the ECMWF[2] forecast large-scale fields.

In order to introduce realistic perturbations in the ensemble prediction system, a potential vorticity error climatology is calculated. This climatology provides the displacement and intensity error of the potential vorticity field in the Mediterranean region.

The potential vorticity error climatology is based on a large collection of MEDEX cyclones. The Mediterranean Experiment on Cyclones that produce High Impact Weather in the Mediterranean, MEDEX, is an European project designed to contribute to the better understanding and short-range forecasting of high impact weather events in the Mediterranean, mainly heavy rain and strong winds, and is focused on Mediterranean cyclones that produce high impact weather.

This masters final thesis is developed in the framework of PRECIOSO, a Spanish project devoted to improve the short and mid-range numerical forecasts of cyclones.

[2]ECMWF as European Centre for Medium-Range Weather Forecasts

Some of the main objectives of PRECIOSO are:

- Design of dynamical techniques for weather forecasting based on the generation of mesoscale ensembles using the nonhydrostatic MM5 model under varying physical parameterizations and initial conditions.
- Design of statistical techniques for the postprocess of meteorological numerical outputs in order to obtain improved precipitations fields (superensemble method, analogue procedure and neuronal network).
- Operational (daily) implementation of the above techniques.

This study is organized as follows: chapter 2 provides a description of relevant concepts for the formulation of this work. In the same chapter, the MM5 numerical model is described. In chapter 3 the potential vorticity error climatology is developed. Chapter 4 describes its application to a Mediterranean cyclogenesis event, and in chapter 5 the study conclusions and further work are discussed.

Chapter 2

Previous Concepts and meteorological tools

2.1 Potential Vorticity Thinking

Mainly owning to historical issues, the use of pressure as the vertical coordinate to describe the atmosphere is the most common, but is not the only one. Other vertical coordinates obtained combining various variables have more useful properties, but can be less intuitive. The potential temperature, θ, is one of this variables and represents the temperature that would acquire a parcel of air at pressure p if adiabatically brought to a standard reference pressure p_0, usually 1000 hPa. Therefore the potential temperature is conserved for all dry adiabatic processes and is given by

$$\theta = T\left(\frac{p_0}{p}\right)^{\frac{R}{C_p}} , \tag{2.1}$$

where T is the current temperature of the parcel, R is the gas constant of air, and C_p is the specific heat capacity at a constant pressure. A coordinate system in which potential temperature is used as vertical coordinate is referred to as an isentropic coordinate system, because contours of equal potential temperature are characterized by equal amounts of specific entropy. Isentropic coordinates are useful because as a first approximation the atmospheric motion is adiabatic, the vertical motion can be shown explicitly in a quasi-horizontal isentropic chart, and the isentropic flow presents a truer picture of the three-dimensional air motion than isobaric surfaces. On the other hand, the atmosphere is not completely adiabatic, especially in the boundary layer and in the vicinity of strong vertical mixing or convection, the isentropic surfaces may intersect the ground, and the meteorologists are unaccustomed to interpreting isentropic weather maps (Carlson, 1991).

The possible advantages of using isentropic coordinates instead of isobaric coordinates lead to search a different approach in the atmosphere diagnostic framework. The desire to develop a formalism in terms of conserved quantities that carry relevant dynamical information of the system raises. The vorticity is a microscopic measure of rotation in a fluid that can be conserved is some atmospheric situation. Thus, vorticity would be used as the first guess to develop this new formalism.

In general, the dynamic meteorology is only concerned with the vertical components of absolute and relativity vorticity, given by the curl of the absolute and relative velocity, respectively:

$$\eta \equiv \vec{k} \cdot \nabla \times \vec{U_a} \ , \tag{2.2}$$

$$\zeta \equiv \vec{k} \cdot \nabla \times \vec{U} \ . \tag{2.3}$$

The vertical component of relative vorticity ζ is highly correlated with synoptic scale weather disturbances. In fact, large positive ζ tends to occur in association with cyclonic storms in Northern Hemisphere. Furthermore, η tends to be conserved following the motion in the middle troposphere (Holton, 1979). The physical interpretation of the ζ can be expressed like the sum of two effects: the rate of change of wind speed normal to the direction of the flow, called shear vorticity, and the turning of the wind along a streamline, called the curvature vorticity.

The study of the vorticity in the isentropic coordinates leads to define a new variable called Potential Vorticity (PV). For a hydrostatic atmosphere, with potential temperature as a the vertical coordinate the Ertel's potential vorticity is given by

$$q = \frac{1}{\rho} \vec{\eta} \cdot \vec{\nabla} \theta \ , \tag{2.4}$$

which is conserved following three-dimensional, adiabatic, frictionless motion (Ertel, 1942). Here $\vec{\eta}$ is the absolute vorticity vector, θ the potential temperature, and ρ the density. In essence, the potential vorticity is proportional to the product of vorticity and stratification that, following a parcel of air, can only be changed by diabatic or frictional processes.

The potential vorticity is an important and very used variable in modern dynamic meteorology basically because of,

1. *Conservation Principle*: for adiabatic and frictionless motion the potential vorticity is conserved, and is well known that a great number of meteorological processes can be considered frictionless and adiabatic.

An increase of stability means a decrease of vorticity, and vice versa. The potential vorticity represents the vorticity that would potentially manifest an air parcel if it were brought adiabatically and without friction to a standard latitude and static stability.

2. *Invertibility Principle*: given the proper boundary conditions and the balance condition[1] imposed on the wind, it is possible to determine, uniquely, the distribution of both vorticity and static stability associated with a PV field. In other words, if the distribution of PV is known, then the wind and temperature fields are also known (Bluestein, 1993).

This other way of looking at the atmosphere dynamics will not necessarily result in new conclusions. However, it may give new dimensions to things that in fact were already known. For example, the traditional way of describing the tropopause is with use of the potential temperature or static stability. This is only a thermodynamical way of characterizing the tropopause. The benefit of using PV is that the tropopause can be understood in both thermodynamic and dynamic terms.

In most of the literature the 2 PVU[2], which separates tropospheric from stratospheric air, is referred to as dynamical tropopause. An abrupt folding or lowering of the dynamical tropopause can also be called an upper PV-anomaly. When this occurs, stratospheric air penetrates into the troposphere resulting in high values of PV with respect to the surroundings, creating a positive PV-anomaly. In the lower levels of the troposphere, strong baroclinic[3] zones often occur which can be regarded as low level PV-anomalies. Under the assumption of a three dimensional balance between the fields of mass (potential temperature), pressure and wind, positive PV-anomalies are connected with cyclonic vorticity and negative PV anomalies with anticyclonic vorticity (Hoskins et al., 1985).

– In the case of a positive PV-anomaly, the isentropes are characterized by higher values than in the surrounding areas above the anomaly (indicating warmer air) and lower values below (indicating colder air). The height of the tropopause has a local minimum. The corresponding pressure and wind field shows an area with low pressure and a cyclonic circulation (Fig. 2.1a).

[1] The balance condition links the wind field to the temperature field .

[2] PVU means potential vorticity unit. 1 PVU = $10^{-6}\mathrm{m}^2\mathrm{s}^{-1}\mathrm{Kkg}^{-1}$

[3] A baroclinic atmosphere is one for which the density depends on both the temperature and the pressure.

– In the case of a negative PV-anomaly, the isentropes are characterized by lower values than in the surrounding areas above the anomaly (indicating colder air) and lower values below (indicating warmer air). The height of the tropopause has a local maximum. The corresponding pressure and wind field shows an area with high pressure and an anticyclonic circulation (Fig. 2.1b).

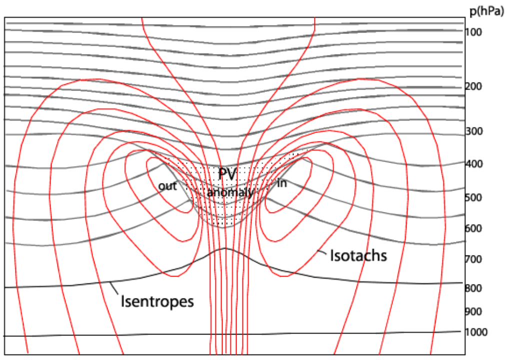

(a) *Positive PV anomaly*

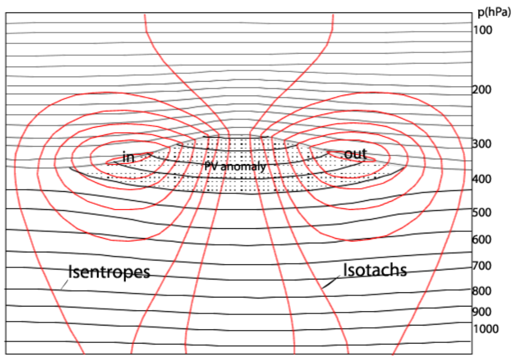

(b) *Negative PV anomaly*

Figure 2.1. *Circularly symmetric flows induced by simple, isolated, PV-anomalies, whose locations are shown stippled. In (a) the sense of azimuthal wind is cyclonic and in (b) it is anticyclonic. Figure from Hoskins et al. (1985).*

The upper PV-anomaly perturbs the wind and pressure fields throughout the whole depth of the troposphere (Fig. 2.1). The effect of this perturbation is proportional to the horizontal scale of the anomaly and inversely proportional to static stability. Observations and model fields show the existence of low level PV-anomalies. These low levels PV-anomalies do not have stratospheric origin but are being formed in strong baroclinic zones where much release of latent heat takes place.

The material conservation, combined with the advantage of invertibility is very useful to describe complex dynamic processes. For example, cyclogenesis can be explained by an interaction between low and upper level PV-anomalies. When the phase difference between two PV-anomalies has an optimum value, interaction followed by mutual amplification takes place. Of course the opposite can also occur, in the case of decaying cyclones.

If an upper level PV-anomaly develops, then as a consequence of the PV conservation, positive vorticity is released and high PV values from the stratosphere influence the less stable environment of the troposphere. The figure 2.2 describes a situation where an originally small-scale upper level

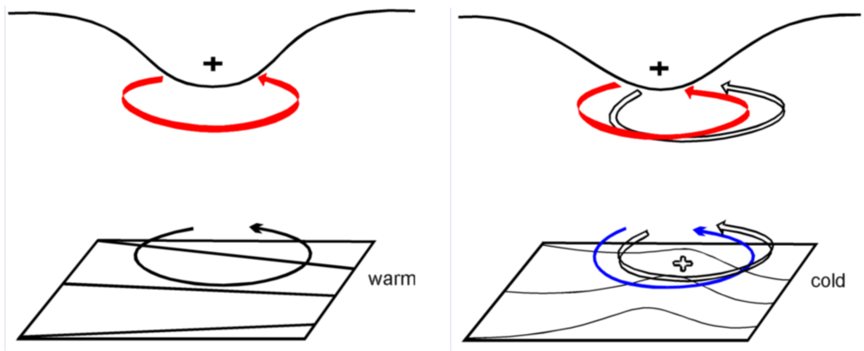

(a) (b)

Figure 2.2. *A schematic picture of cyclogenesis associated with the arrival of an upper air PV-anomaly over a low-level baroclinic region. In (a) the upper air cyclonic PV-anomaly, indicated by solid plus sign and associated with the low tropopause shown, has just arrived over a region of significant low-level baroclinicity. The circulation induced by the anomaly is indicated by solid arrows, and potential temperature contours are shown on the ground. The low-level circulation is shown above the ground for clarity. The advection by this circulation leads to a warm temperature anomaly somewhat ahead of the upper PV-anomaly as indicated in (b), and marked with an open plus sign. This warm anomaly induces the cyclonic circulation indicated by the openarrows in (b). If the equatorward motion at upper levels advects high-PV polar lower-stratospheric air, and the poleward motion advects low-PV subtropical upper-tropospheric air, then the action of the upper-level circulation induced by the surface potential temperature anomaly will, in effect, reinforce the upper air PV anomaly and slow down its eastward progression. Figure from Hoskins et al. (1985).*

trough moves over a zonally oriented surface cold front when an upper-level, positive PV-anomaly, is being advected over a zone of strong low-level equatorward temperature gradient. The left figure (a) shows such a situation with the solid plus sign indicating the upper level PV-anomaly. The thick solid arrow around the PV maximum indicates the cyclonic rotation. This rotation is induced at lower levels of the baroclinic zone as shown by the thin solid circulation arrow. This low level circulation causes warm advection ahead leading to a low level positive temperature anomaly indicated by the open plus sign in the right figure (b). This temperature anomaly is associated with a cyclonic vortex which is marked by the open arrow at low levels. In turn, this circulation has a positive feedback to the upper troposphere, shown by an open circulation arrow at higher levels. In parallel a second process is taking place, the induced low level vortex results in a strong equatorward wind component under the upper level PV-anomaly. This southward component also influences the higher levels and leads to an equatorward advection of the upper level PV-anomaly which in turn intensifies the upper level wave.

Within this increased flow, higher PV values to the west of the PV-anomaly are advected southward and lower PV values to the east of the PV-anomaly are advected northward. As a consequence of the latter process, the eastward movement of the PV-anomaly is decreased. Hence, the interaction between low and upper level circulations and the already ongoing cyclogenesis process will strengthen.

2.2 Potential Vorticity Inversion Technique

The invertibility principle can be applied to develop a diagnostic system that obtains the wind and temperature perturbations associated with a given PV perturbation distribution. This application is called potential vorticity inversion technique and can be very useful in order to discuss the relevance of the PV-anomalies in the atmospheric behavior (Romero, 2001). For example, the PV inversion technique allows to diagnose developments in which the PV-anomalies are not growing, but are merely changing their relative positions or their shapes. Furthermore, the conservation law for PV will help isolate those disturbances growing chiefly by nonconservative processes while the invertibility principle allows direct calculation of their associated circulation.

The potential vorticity inversion technique, developed by Davis and Emanuel (1991), uses the balance condition derived by Charney (1955) to link the wind field to the temperature field. This balance condition is very accurate in flows with large curvature because is quite similar to gradient wind balance. The Charney balance equation is obtained taking the horizontal divergence of the horizontal momentum equations and decomposing the wind field into a nondivergent and an irrotational part. After an scaling, the resulting equation may be written in spherical coordinates (λ, ϕ, a)

$$\nabla^2\Phi = \nabla \cdot (f\nabla\Psi) + \frac{2}{a^4\cos^2\phi}\frac{\partial\left(\frac{\partial\Psi}{\partial\lambda}, \frac{\partial\Psi}{\partial\phi}\right)}{\partial(\lambda, \phi)} \ , \tag{2.5}$$

with Φ the geopotential, Ψ the nondivergent stream function, λ the longitude, ϕ the latitude, and a the earth's radius. Relation (2.5) reduces to geostrophic balance if f is constant and the Jacobian term is neglected.

One more diagnostic equation relating Ψ to Φ is needed in order to close the system. This is obtained from an approximate definition of Ertel's Potential Vorticity (ErPV):

$$q = -\frac{g\kappa\pi}{p}\left(\eta\frac{\partial\theta}{\partial\pi} - \frac{1}{a\ \cos\phi}\frac{\partial v}{\partial\pi}\frac{\partial\theta}{\partial\lambda} + \frac{1}{a}\frac{\partial u}{\partial\pi}\frac{\partial\theta}{\partial\phi}\right) \ , \tag{2.6}$$

where $\kappa = R_d/C_p$, p is the pressure, π is the Exner function $[C_p(p/p_0)^\kappa]$ and serves as vertical coordinate, η is the vertical component of absolute vorticity and the hydrostatic approximation has been made. Performing an scaling of (2.6) results in a relation between the potential vorticity, Φ and Ψ,

$$q = -\frac{g\kappa\pi}{p}\left[\left(f+\nabla^2\Psi\right)\frac{\partial^2\Phi}{\partial\pi^2} - \frac{1}{a^2\cos^2\phi}\frac{\partial^2\Psi}{\partial\lambda\partial\pi}\frac{\partial^2\Phi}{\partial\lambda\partial\pi} - \frac{1}{a^2}\frac{\partial^2\Psi}{\partial\phi\partial\pi}\frac{\partial^2\Phi}{\partial\phi\partial\pi}\right] . \quad (2.7)$$

The approximation used here replaces the vertical derivative of the total wind by the vertical derivative of the nondivergent wind. Equations (2.5) and (2.7) form a complete system for the unknowns Φ and Ψ, given q.

For boundary conditions, Φ and Ψ are defined in the lateral boundaries and their vertical derivatives on the horizontal boundaries are specified. The observed geopotential serves as Φ on the lateral edges and $\partial\Phi/\partial\pi = -\theta$ is applied at the top and bottom. The gradient of Ψ along the edge is forced to match the normal wind component, and the horizontal boundaries are given by $\partial\Psi/\partial\pi = -\theta$, applied at both the top and the bottom. The obtained solutions are fairly insensitive to this choice of boundary conditions.

The technique used to solve the system is an iterative numerical method of successive overrelaxation (SOR) applied to each vertical level. As long as the ErPV is everywhere positive the method consistently converged. Tests with different initial guesses showed that the solution obtained was apparently unique, or at least other existing solutions were unreachable.

2.3 Mesoscale Atmospheric Model

The atmosphere is ruled by complex non-linear dynamical processes. Due to this non-linearity, the dynamical equations can not be resolved analytically. Therefore, the necessity of developing a numerical model capable of describing these non-linear processes rises. Nowadays, a large number of atmospheric models have been designed and are being used regularly. These models use parameterizations to describe the atmospheric process.

The non-hydrostatic mesoscale MM5 model is a high resolution short-range weather forecast model developed by the National Center for Atmospheric Research (NCAR) and the Pennsylvania State University (PSU) (Dudhia, 1993; Grell et al., 1995). The main characteristics of the MM5 are described below. The model user must decide which of these characteristics should be used to run the desired simulation. In this study a single computational domain with nonhydrostatic dynamics with meteorological grid data (FDDA of observations is not included) is used. The specific characteristics of the study simulations are explained in the next chapter.

(i) The MM5 model horizontal and vertical grid

The MM5 acquires and analyzes the data on pressure surfaces. This information has to be interpolated to the model's vertical coordinate, σ, before being used. The vertical coordinate σ is terrain following, like figure 2.3 shows, meaning that the lower grid levels follow the terrain while the upper surface is flat. The vertical coordinate σ is defined by

$$\sigma = \frac{p - p_0}{p_s - p_t} \ , \tag{2.8}$$

where p_0 is the reference-state pressure, p_t is a specified constant top pressure, and p_s is the reference-state surface pressure. The values of σ go from 0 at the atmosphere's top to 1 at the earth's surface.

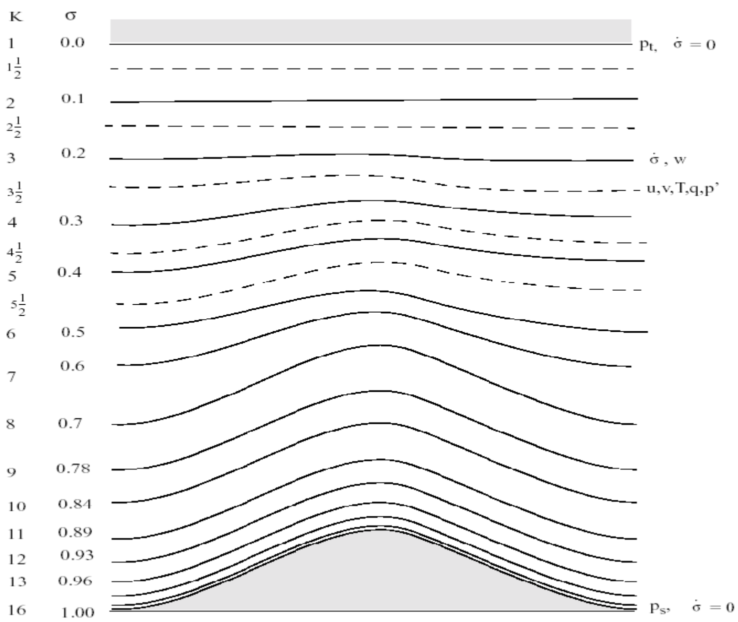

Figure 2.3. *Schematic representation of the vertical structure of the model. This example is for 15 vertical layers. Dashed lines denote half-sigmalevels, solid lines denote full-sigma levels.*

The horizontal grid has an Arakawa-Lamb B-staggering of the velocity variables with respect to the scalars. This is shown in figure 2.4 where it can be seen that the scalars, like temperature, are defined at the center of the grid square, while the eastward and northward velocity components are collocated at the corners. All these variables are defined in the middle of each model vertical layer, referred to as half-levels, and vertical velocity is carried at the full levels.

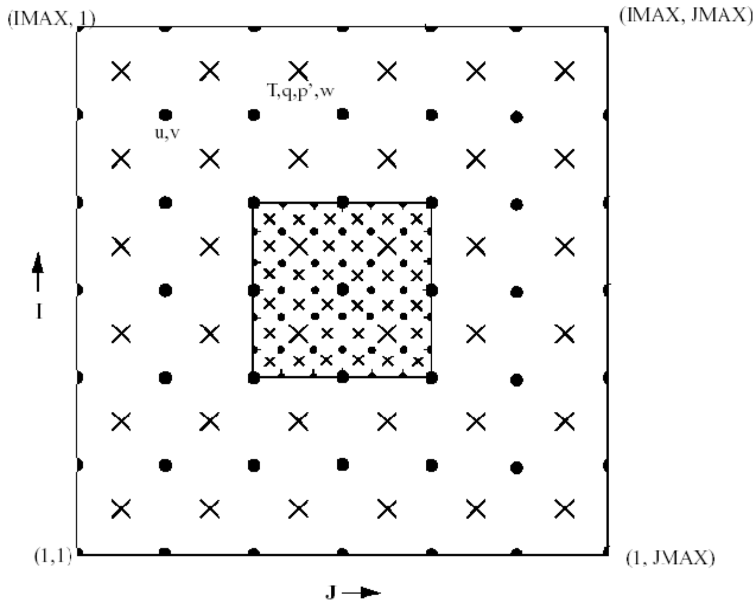

Figure 2.4. *Schematic representation of the horizontal Arakawa-Lamb B-staggering staggering of the dot and cross grid points. The smaller inner box is representative mesh staggering for a 3:1 coarse-grid distance fine-grid distance ratio.*

(ii) The nesting capability

The MM5 model contains a capability of multiple nesting with up to nine domains running at the same time and completely interacting. A possible configuration is shown in figure 2.5. The nesting ratio is always 3:1 for two-way interaction, and is not restricted for one-way nesting. The one-way nesting differs from two-way nesting in having no feedback and coarser temporal resolution at the boundaries. Each sub-domain has a mother domain in which it is completely embedded. Moving a domain and turn on and off a nest at any time in the simulation is also possible. There are three ways of doing two-way nesting. First, nest interpolation, where the nest is initialized by interpolating coarse-mesh fields and requires no additional input files. Second, nest analyses input, which requires a model input file to be prepared for the nest in addition to the coarse mesh. Third, nest terrain input that requires just land-use input file, so the meteorological fields are interpolated from the coarse mesh and vertically adjusted to the new terrain (land-use).

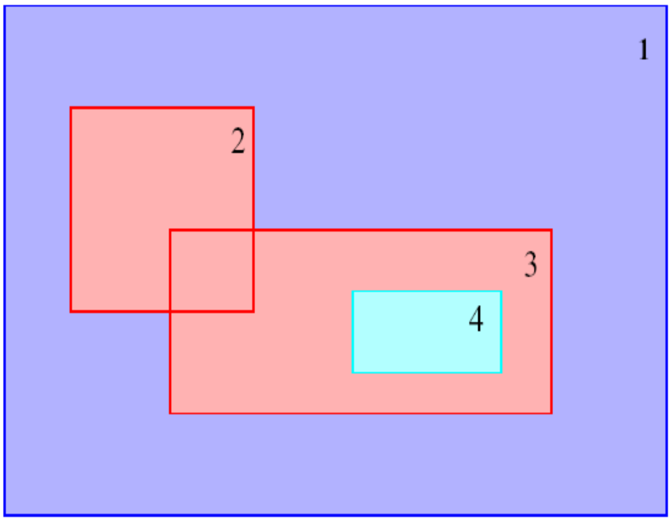

Figure 2.5. *Example of nesting configuration. The shading shows three different levels of nesting.*

(iii) The lateral boundary conditions

A regional numerical weather prediction model requires lateral boundary conditions. In MM5 all four boundaries have specified horizontal winds, temperature, pressure and moisture fields, and can have specified microphysical fields, such as cloud and precipitation species, if these are available. These boundary values have to be set in the simulations in addition to initial values for these fields.

The boundary values can come from analyses at the future times, from a previous coarser-mesh simulation, and from another model's forecast. For real-time forecasts the lateral boundaries will ultimately depend on a global-model forecast. In studies of past cases the analyses providing the boundary conditions may be enhanced by observation analysis in the same way as initial conditions are. The MM5 uses these discrete-time analyses by linearly interpolating them in time to the model time. In two-way nest, the boundaries are updated every coarse-mesh timestep.

(iv) The nonhydrostatic dynamics

In the mesoscale models, the hydrostatic approximation can be applied when the typical horizontal grid sizes are comparable with or greater than the vertical depth of features of interest. Then, the pressure is completely determined by the overlying air's mass, like the hydrostatic relation shows,

$$dz = -\rho_0 g \; dz \; . \tag{2.9}$$

However, when the scale of resolved features in the model have aspect ratios nearer unity, or when the horizontal scale becomes shorter than the vertical scale, nonhydrostatic dynamics can not be neglected. The nonhydrostatic dynamic introduces an additional term, the vertical acceleration that contributes to the vertical pressure gradient, so the hydrostatic balance is no longer exact.

(v) The reference state in the nonhydrostatic model

The reference state is an idealized temperature profile in hydrostatic equilibrium, given by

$$T_0 = T_{s0} + A \; ln \left(\frac{p_0}{p_{00}} \right) \; , \tag{2.10}$$

where T_0 is specified by: sea-level pressure, p_{00}, the reference temperature at p_{00}, T_{s0}, and a measure of lapse rate, A, representing the temperature difference between p_{00} and p_{00}/e. Usually, just T_{s0} needs to be selected based on a typical sounding in the domain.

The surface reference pressure, therefore, depends entirely upon the terrain height, and can be derived from eq. (2.10), using the hydrostatic relation (2.9),

$$Z = -\frac{RA}{2g} \left(ln \frac{p_0}{p_{00}} \right)^2 - \frac{RT_{s0}}{g} \left(ln \frac{p_0}{p_{00}} \right) \tag{2.11}$$

and this quadratic can be solved for p_0(surface) given the terrain elevation, Z. Once this is done, the heights of the model σ levels are found from

$$p_0 = p_{s0}\sigma + p_{\text{top}} \; , \tag{2.12}$$

where

$$p_{s0} = p_0(\text{surface}) - p_{\text{top}} \; , \tag{2.13}$$

and then eq. (2.11) is used to find Z from p_0. It can be seen that since the reference state is independent of time, the height of a given grid point is constant.

(vi) The four-dimensional data assimilation

The four-dimensional data assimilation (FDDA) allows to input data over an extended time period to the model. Essentially FDDA allows the model to be run with forcing terms that guide the model towards the observations or analyses. The benefit of this is that after a period of nudging the model has been fit to some extent to all the data over that time interval while also remaining close to a dynamical balance. This has advantages over just initializing with analyses at a single synoptic time because adding data over a period effectively increases the data resolution.

The two primary uses for FDDA are dynamical initialization and four dimensional datasets. Dynamical initialization is where FDDA is used over a pre-forecast period to optimize the initial conditions for a real-time forecast. The second application, four-dimensional datasets, is a method of producing dynamically balanced analyses that have a variety of uses from budget to tracer studies. The model maintains realistic continuity in the flow and geostrophic and thermal-wind balances while nudging assimilates data over an extended period.

(vii) The land-use categories

The MM5 provides three sets of land-use categorizations that are assigned along with elevation. These have various categories like: type of vegetation, desert, urban, water, ice, and others. Each grid cell of the model is assigned one of the categories, and this determines surface properties such as albedo, roughness length, longwave emissivity, heat capacity and moisture availability. Additionally, if a snow cover dataset is available, the surface properties may be modified accordingly. These values are also variable according to summer or winter season, for the northern hemisphere. It is important to note that the values are climatological and may not be optimal for a particular case, especially moisture availability.

(viii) The map projections and map-scale factors

The modeling system has a choice of several map projections. Lambert Conformal is suitable for mid-latitudes, Polar Stereographic for high latitudes and Mercator for low latitudes. These transformations are accounted for in the model pre-processors that provide data on the model grid, and post-processors.

The map scale factor, m, is defined by

$$m = \frac{\text{distance on grid}}{\text{actual distance on earth}} \ , \tag{2.14}$$

and its value is usually close to one varying with latitude. The projections in the model preserve the shape of small areas, but the grid length varies across the domain to allow a representation of a spherical surface on a plane surface. Map scale factors need to be accounted for in the model equations wherever horizontal gradients are used.

(ix) The basic equations of the MM5 model

As expected, the MM5 basic equations are nonhydrostatic and are given in terms of terrain following coordinates (x,y,σ). These equations without moisture terms are given by

- the pressure equation:

  $$\frac{\partial p'}{\partial t} - \rho_0 g\omega + \gamma p \nabla \cdot \overrightarrow{V} = -\overrightarrow{V} \cdot \nabla p' + \frac{\gamma p}{T}\left(\frac{\dot{Q}}{c_p} + \frac{T_0}{\theta_0} D_\theta\right) \ , \tag{2.15}$$

  where p' is the nonhydrostatic perturbed pressure, p is the hydrostatic pressure, ρ_0 is the air density, g is the gravity constant, ω is the vertical velocity, $\gamma = \frac{C_p}{C_v}$, where C_p is the air calorific heat at constant pressure and C_v is at constant volume, $\overrightarrow{V}$ is the velocity vector, $\dot{Q}$ is the heat exchange with the environment, T_0 is the temperature of the buoyancy term, θ_0 is the reference potential temperature and D_θ is the heat loss owning to friction and turbulence. This equations shows that pressure temporal variations are due to the rising and subsidence fluid motions, variations produced by converge and divergence, pressure advection and variations provided by heat exchanges.

– the momentum equations:

a) component x:

$$\frac{\partial u}{\partial t} + \frac{m}{\rho}\left(\frac{\partial p'}{\partial x} - \frac{\sigma}{p^*}\frac{\partial p^*}{\partial x}\frac{\partial p'}{\partial \sigma}\right) = -\overrightarrow{V}\cdot\nabla u$$
$$+ v\left(f + u\frac{\partial m}{\partial y} - v\frac{\partial m}{\partial x}\right) - ew\cos\alpha - \frac{uw}{r_{earth}} + D_u \ , \quad (2.16)$$

where m is the map scale factor, $p^* = p_{surface} - p_{top}$ is the difference between pressure, f and $e = 2\Omega\cos\lambda$ are the Coriolis terms where λ is the latitude, $\alpha = \phi - \phi_c$, ϕ is the longitude and ϕ_c is the central longitude, $u\frac{\partial m}{\partial y}$, $v\frac{\partial m}{\partial x}$ and r_{earth} are the curvature effect terms, and D_u is the heat loss term due to friction and turbulence in the component x direction. The component x momentum temporal variations are due to spacial variations in the pressure field, u velocity advection and curvature and Coriolis effects.

b) component y:

$$\frac{\partial v}{\partial t} + \frac{m}{\rho}\left(\frac{\partial p'}{\partial y} - \frac{\sigma}{p^*}\frac{\partial p^*}{\partial y}\frac{\partial p'}{\partial \sigma}\right) = -\overrightarrow{V}\cdot\nabla v$$
$$+ u\left(f + u\frac{\partial m}{\partial y} - v\frac{\partial m}{\partial x}\right) + ew\sin\alpha - \frac{uw}{r_{earth}} + D_v \ . \quad (2.17)$$

c) component z:

$$\frac{\partial w}{\partial t} - \frac{\rho_0}{\rho}\frac{g}{p^*}\frac{\partial p'}{\partial \sigma} + \frac{g}{\gamma}\frac{p'}{p} = -\overrightarrow{V}\cdot\nabla w + g\frac{p_0}{p}\frac{T'}{T_0}$$
$$- \frac{gR_d}{c_p}\frac{p'}{p} + e(u\cos\alpha - v\sin\alpha) + \frac{u^2+v^2}{r_{earth}} + D_w \ , \quad (2.18)$$

where R_d is the dry air universal constant.

– the thermodynamic equation:

$$\frac{\partial T}{\partial t} = -\overrightarrow{V}\cdot\nabla T$$
$$+ \frac{1}{\rho C_p}\left(\frac{\partial p'}{\partial t} + \overrightarrow{V}\cdot\nabla p' - \rho_0 g w\right) + \frac{\dot{Q}}{C_p} + \frac{T_0}{\theta_0}D_\theta \ . \quad (2.19)$$

The temperature temporal variations are due to thermal advection, density variations, heat exchanges and heat loss owning to friction and turbulence.

2.4 Probabilistic Forecasting

The numerical models used in operational and research centers will predict realistic weather features, but the errors in a forecast will inevitably grow with time due to the chaotic nature of the atmosphere. In fact it is known that, due to the nonlinear nature of fluid dynamics, it is impossible to accurately predict the state of the atmosphere (Lorenz, 1963). Furthermore, existing observation networks have limited spatial and temporal resolution which introduces uncertainty into the calculated initial state of the atmosphere.

To account for this uncertainty, stochastic or ensemble forecasting is used, involving multiple forecasts created with different model systems, different physical parameterizations, or varying initial conditions. In the later, instead of running just a single forecast the model is run a number of times from slightly different starting conditions. The complete set of forecasts is referred to as the ensemble and individual forecasts within it as ensemble members. The initial differences between ensemble members are very small so that if members are compared with observations it would be impossible to say which members fitted the observations better. All members are therefore equally likely to be correct, but several days ahead the forecasts can be quite different (Fig. 2.6).

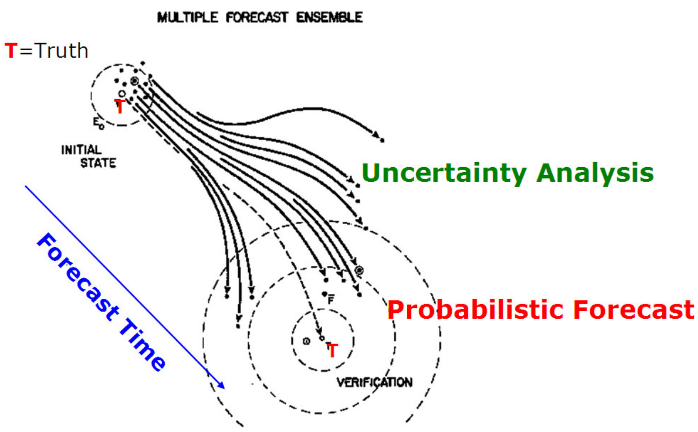

Figure 2.6. *The Ensemble Prediction System allows to sample several potential future states of the system by perturbing the initial conditions according to the uncertainties associated with observations. A statistical analysis could be used to discern likely conditions, average conditions, and a range of uncertainties associated with the predictions.*

The Ensemble Forecasting System (EPS) is usually evaluated in terms of the ensemble mean of a forecast variable and the ensemble spread, which represents the degree of agreement between various forecasts in the ensemble system. This probabilistic forecasting has shown better detection skill of extreme events that deterministic forecasting (Jordan II, 2005).

An improvement of the EPS is the superensemble forecast method (Krishnamurti et al., 1999, 2000a,b, 2001). The superensemble statistical method employs past forecasts from a group of ensemble members in an effort to correct biases[4] in these forecasts and rank the relative strength of each of the member (training phase). Then, the superensemble prediction is derived using the data gathered through the training phase and current ensemble members forecasts (forecast phase). A schematic view of operational application of the superensemble is shown in figure 2.7.

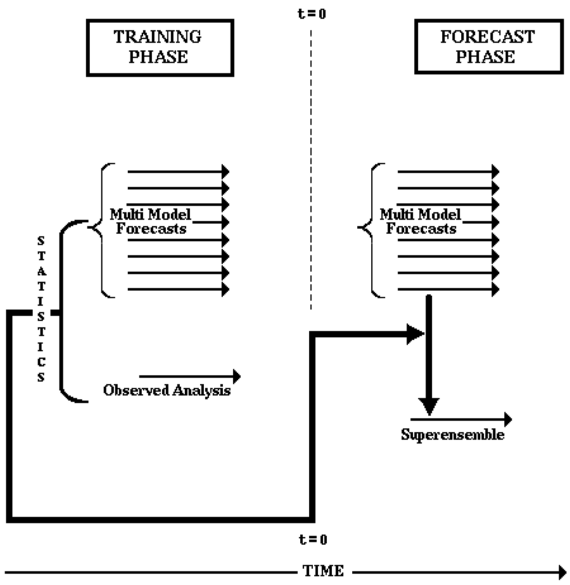

Figure 2.7. *The vertical line in the center denotes time $t = 0$, and the area to the left denotes the training area where a large number of forecasts experiments are carried out by multianalysis-multimodel system. During the training period, the observed fields provide statistics that are then passed on to the area on the right, where $t > 0$. Here the multianalysis-multimodel forecasts along with the aforementioned statistics provide the superensemble forecasts. Figure from Krishnamurti et al. (2001).*

[4]The bias is a term which refers to how far the average statistic lies from the parameter it is estimating, that is, the error which arises when estimating a quantity.

Chapter 3

Potential vorticity error climatology

The designed ensemble prediction system is based on perturbed initial and boundary conditions through the potential vorticity field. Then, in order to introduce realistic perturbations a potential vorticity error assessment has to be done.

In a previous step, the data source needs to be decided. The main goal of designing this EPS for the Mediterranean area is to be able to predict extreme events. Therefore, the EPS needs to be a real time operating system. This means that the meteorological analyses fields can not be the data source. This is because the analyses are a weighted compromise between observations and an atmospheric first guess (usually a 6 hour forecast), so they are not available for future times. Therefore, the most logical data source for real-time purpose would be the meteorological forecast fields. It is necessary to emphasize that all the meteorological data is provided by the European Centre for Medium-Range Weather Forecasts, ECMWF.

The potential vorticity error climatology (PVEC) is calculated comparing ECMWF 24 h forecast and ECMWF analyses PV fields, assuming the analyses PV fields as the best available atmospheric description. It is assumed too that the main error sources are the possible displacement between the 24 h forecast and ECMWF analyses PV fields and the difference in PV intensity. All computations and statistics are done for a collection of 19 MEDEX cyclones briefly described in appendix A, and for the ECMWF standard pressure levels[1].

[1]ECMWF standard pressure levels: 100, 200, 300, 400, 500, 700, 850, 925 and 1000 hPa

The PVEC has been done following the next steps, for each pressure level.

1. Obtain the ECMWF 24 h forecast and ECMWF analyses PV fields for the MEDEX cyclones collection.
2. Determine the PV displacement error.
3. Determine the PV intensity error.
4. Calculate the percentiles of the displacement and intensity error.
5. Fit analytical functions to the percentiles of the displacement and intensity error.

These steps are detailed below.

3.1 Obtain the PV fields

The area of study is defined as a 22.5 km resolution domain centered in 39.8 lat. and 2.4 lon., with a 120x120 grid. This domain contain all the areas affected by the selected MEDEX cyclones and corresponds to the Domain 1 (Fig. 3.1) used in the deterministic operative model run by UIB Meteorology Group (`http://mm5forecasts.uib.es`) .

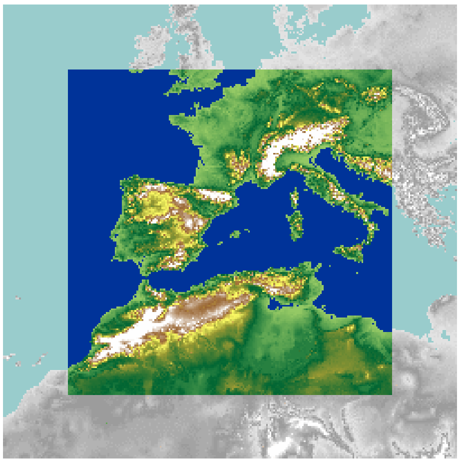

Figure 3.1. *Domain 1 of the UIB Meteorology Group operative model*

The PV fields of the analyses and forecast data are calculated every 6 h for all the days contained in the cyclone collection, plus the day before of each event. Furthermore, the calculations are done using the Ertels's PV definition given in eq. (2.7), for the defined domain.

3.2 Displacement error

It is likely that the 24 h forecast fields are displaced backward or forward respect to the analyses fields. This lag can be minimized displacing the 24 h forecast fields to obtain maximum correlation with the analyses fields. To obtain this displacement error, the following method is applied.

A matrix of 21x21 grid point associated to its central point is defined (in distance 450x450 km^2). Then, each grid point of the 24 h forecast PV field is displaced in all directions up to 10 grid points (225 km is the typical distance between PV structures, and so it is chosen to be sure of capture the lag). Due to the dimensions of the matrix associated to each grid point the boundary can not be evaluated. In each of these displacements the correlation between the 24 h forecast displaced matrix and the respective analyses matrix is calculated. The matrix dimension, 450x450 km^2, assures that obtained correlation reflects whether it is really the same structure or a different one, due to the typical scales of the PV fields. Then, the displacement error (DE) corresponds to the minimum displacement of the 24 h forecast PV field showing local maximum correlation with the analyses PV field. The figure 3.2 shows a very simple example of this method.

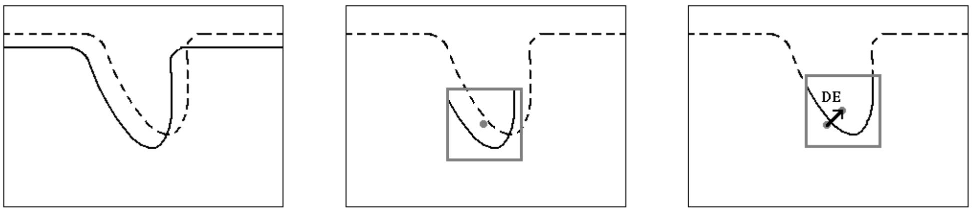

(a) (b) (c)

Figure 3.2. *A very simple example of how the displacement error is calculated. (a) Initial spatial pattern of the 24 h forecast (solid line) and analysis (dashed line) PV fields,(b) Area of 24 h forecast PV field associated to a selected grid point of the study domain, (c) Minimum displacement of the 24 h forecast PV field showing local maximum correlation with the analysis PV field.*

The displacement error is a discrete magnitude due to its own definition. The representation of the number of grid points as function of the displacement error, displacement density function, shows a very clear symmetry along South-North and West-East directions (Fig. 3.3). This fact allows to use an absolute value in both directions. Furthermore, the displacement error shows a lack of dependence on the PV value of the grid (Fig. 3.5).

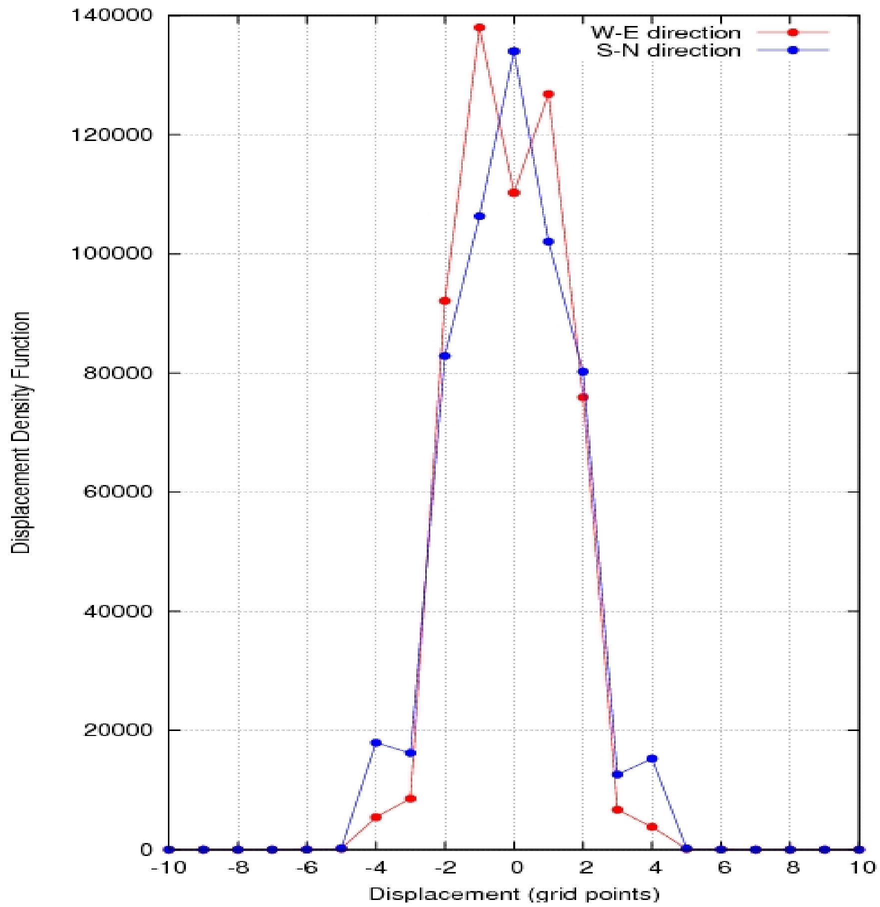

Figure 3.3. *This figure corresponds to the displacement density function at 300 hPa, and represents the number of grid points as function of the displacement error. The South-North (blue line) and West-East (red line) directions are represented separately. The negative values represent the displacement in the opposite way along its direction.*

3.3 Intensity error

The intensity error corresponds to the difference between the displaced 24 h forecasts PV fields and analyses PV fields. The intensity error of each grid point is calculated as follows:

1. determine the 21x21 grid points matrix associated,
2. calculate the difference between the displaced 24 h forecasts and the analyses for all these grid points,
3. calculate the average of this difference.

Then, this average is the called intensity error (IE). This error presents a very high symmetry between positive and negative values, so the absolute value is used. Furthermore, the intensity error shows a clear dependence on the PV value of the grid (Fig. 3.4).

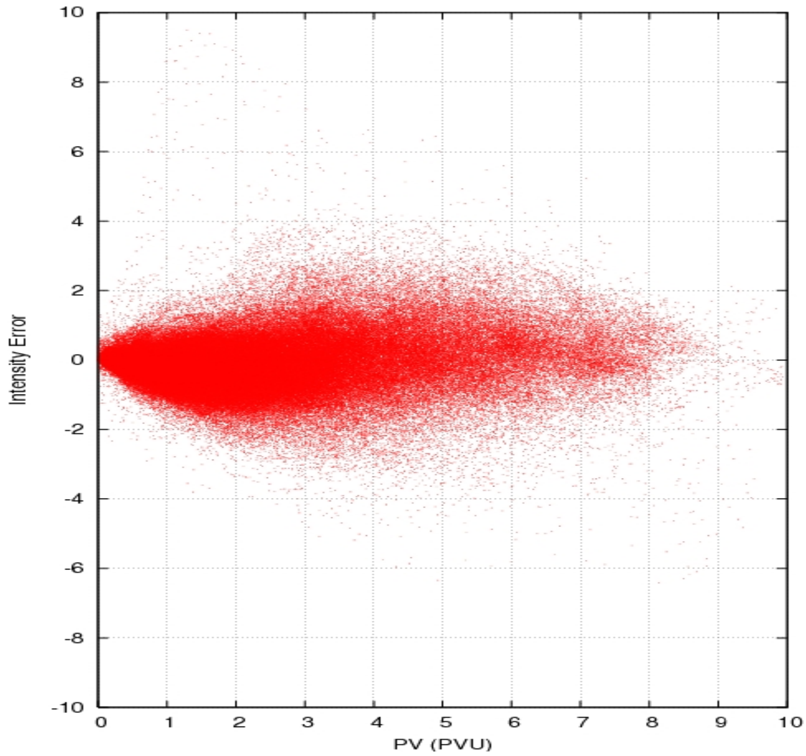

Figure 3.4. *Intensity error at 300 hPa. Presents a very high symmetry and a clear dependence on the PV value.*

With the purpose of incorporate this dependence on the PV value a new variable based on the intensity error is defined. The %IE is defined as $\frac{\text{intensity error}}{\text{analysis PV}}\%$.

3.4 Displacement and intensity error percentiles: fitted analytical functions

In order to obtain the distribution of the PVEC, the percentile of these errors, DE and %IE, are calculated. This percentile gives information about the value of a variable below which a certain percent of observations fall. So, for example, the 20th percentile is the value below which 20 percent of the observations are found.

Before the percentile is calculate, all the values are separated by values of analysis PV in classes of 0.1 PVU for each pressure level. But, since the DE is not continuous, the percentile cannot be calculated with the traditional method. The designed method takes advantage of the lack of dependence on the PV value.

The method consists of calculating the percentage of grid points with a displacement of X grid points (X goes from 0 to 10 grid points). Now, this percentage is assigned to a DE of X.5 grid points. At this point each DE has a percentage associate but the percentile levels go from 10, 20, to 100 percentage. Then, the percentiles are calculate with a linearly interpolation of the obtained percentages, in other words, the DE associated with each percentiles is fitted linearly. A brief schematical description is shown bellow:

1. Calculate the percentage of grid points with a displacement of X grid points (X goes from 0 to 10 grid points),
2. this percentage is assigned to a DE of X.5 grid points, and
3. the DE associated with each percentile is fitted linearly.

Analytical functions have been fitted to model the percentile levels of displacement and intensity errors. It should be emphasized that the displacement and intensity error depend on the pressure level. The fitted functions are a linear-like function for each direction of the DE (Fig. 3.5), and a potential-like function as $\%\mathrm{IE}(\mathrm{PV}) = a \cdot \mathrm{PV}^{b} + c$ for the %IE (Fig. 3.6).

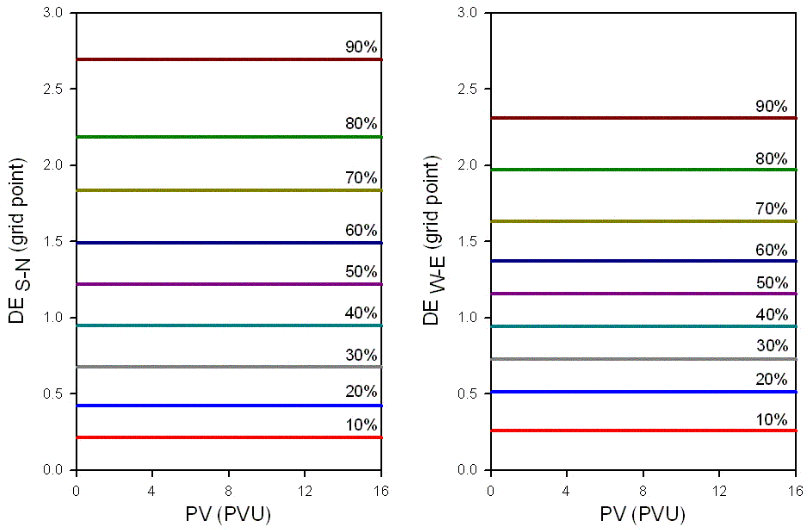

Figure 3.5. *The DE percentile levels along South-North and West-East direction at 300 hPa*

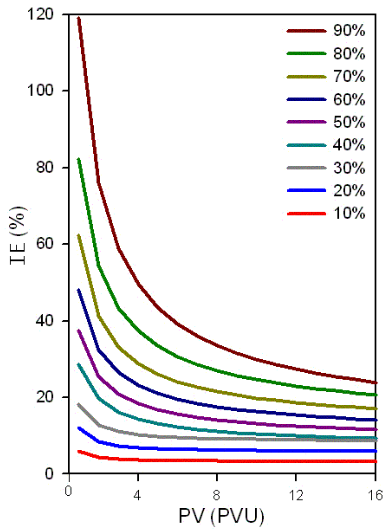

Figure 3.6. *The %IE percentile levels at 300 hPa*

Chapter 4

Application to Mediterranean cyclogenesis events

Once the PVEC is obtained, it is used to define the EPS members. The ensemble members are the original state and several perturbed states. This perturbed members are obtained using the following methodology.

4.1 Methodology

The PVEC is used to implement the ensemble system by randomly perturbing the fields. This random approach means that a random number determines the magnitude of the perturbation, in other words, which error percentile level is applied, and another random number determines if the perturbation is positive or negative.

In order to be consistent with the most influential PV structures, these random perturbations are only applied along the zones with the most intense PV values and gradients. The automatic detection of these zones is done following the next steps. It should be noticed that to avoid boundary problems a new domain of 200x200 grid points is defined during this phase.

1. A highly smoothed PV field is calculated.
2. A *pseudo-sensitivity* field is defined as the difference between the original PV field and the smoothed PV field.
3. A threshold is defined for each pressure level as

$$\text{threshold}_k = \frac{1}{nr \cdot nc} \sum_{i,j}^{nr,nc} |\text{pseudo-sensitivity}_{i,j,k}| \;, \tag{4.1}$$

where k is the pressure level, i and j are the x and y coordinates of the grid and nr and nc are the horizontal grid dimensions, respectively.

4. The zones with PV higher and lower than the threshold are detected in the three dimensional big domain. The positive detection area covers approximately half of the of the big domain (200x200 grid points) area.

5. It is assigned the same error percentile level of intensity and displacement to the detected zones that correspond to a same PV structure. This percentile error is different for intensity and for the displacement in each direction. The sign of the intensity error is assigned randomly too, but a uniform randomly selected directional error is assigned to the whole domain to avoid discontinuities in the PV field.

The figure 4.1 shows the zones with the most intense PV values and gradients detected with the method explained above at 300 hPa for the MEDEX cyclone of 9th June 2000.

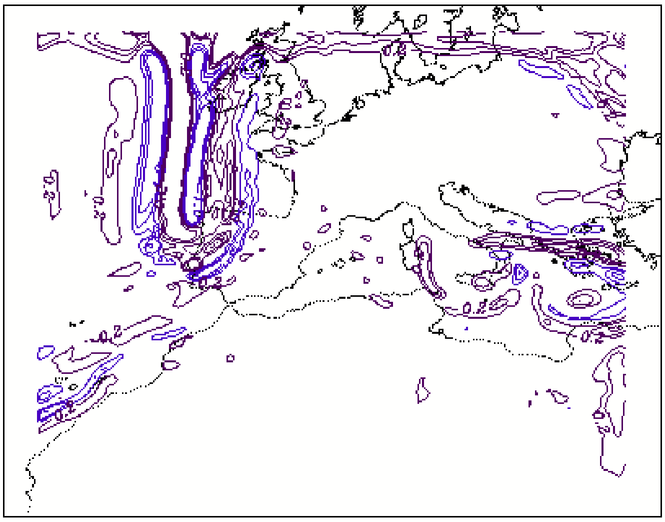

Figure 4.1. *Zones with intense PV values and gradients at 300 hPa for the MEDEX cyclone of 9th June 2000 at 00 UTC. Positive values are in purple and negatives in blue. (Coordinated Universal Time, UTC, is a high-precision atomic time standard.)*

Then, the PVEC converts the percentile levels to PV errors and the PV perturbed field is obtained. The PV inversion technique uses this PV perturbed field to obtain the wind and temperature (mass) perturbed balance fields. Finally, the difference between the original and perturbed balance fields provides the initial and boundary perturbations for each member of the ensemble.

4.2 An illustrative case: MEDEX cyclone of 9th June 2000

The MEDEX cyclone of 9th June 2000 affected the northeastern part of the Iberian Peninsula. The heavy rains produced severe floods over densely populated areas and very heavy material losses. The observed accumulated rainfall over Catalonia is shown in figure 4.2.

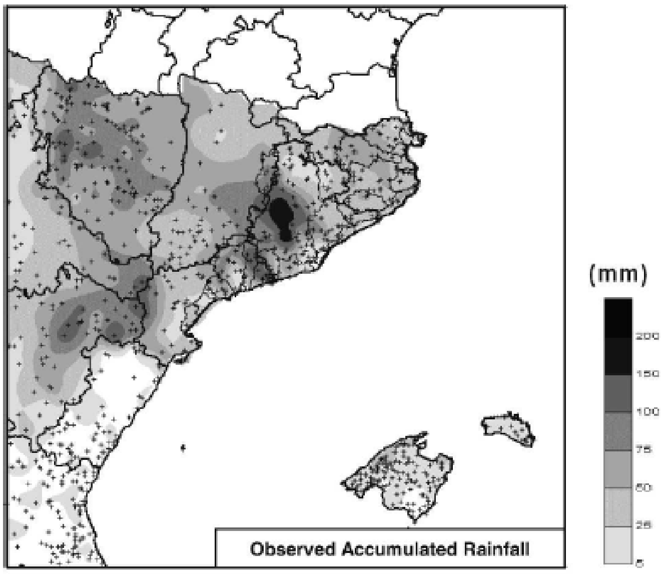

Figure 4.2. *Observed accumulated rainfall (shaded according to scale, mm) between 0700 UTC 9 Jun 2000 and 0700 UTC 11 Jun 2000. Internal basins of Catalonia (thin continuous line) and the provinces of the northeastern Spain and southern France (thick continuous line) are plotted. Maximum value is 223 mm. Rain gauge network (crosses) is highlighted. Figure from Martín et al. (2007).*

The event was characterized by the entrance of an Atlantic low-level cold front and an upper-level trough that contributed to the generation of a mesoscale cyclone in the Mediterranean Sea east of mainland Spain. The circulation associated with this mesoscale cyclone advected warm and moist air toward Catalonia from the Mediterranean Sea. The convergence zone between the easterly flow and the Atlantic front, as well as the complex orography of the region, favored the triggering and organization of the convective systems. Radar showed the development of two long-lived mesoscale convective systems that merged and remained quasi-stationary nearby the city of Barcelona for nearly 2 h. A brief description of the synoptical situation is shown in figure 4.3. (Martín et al., 2007).

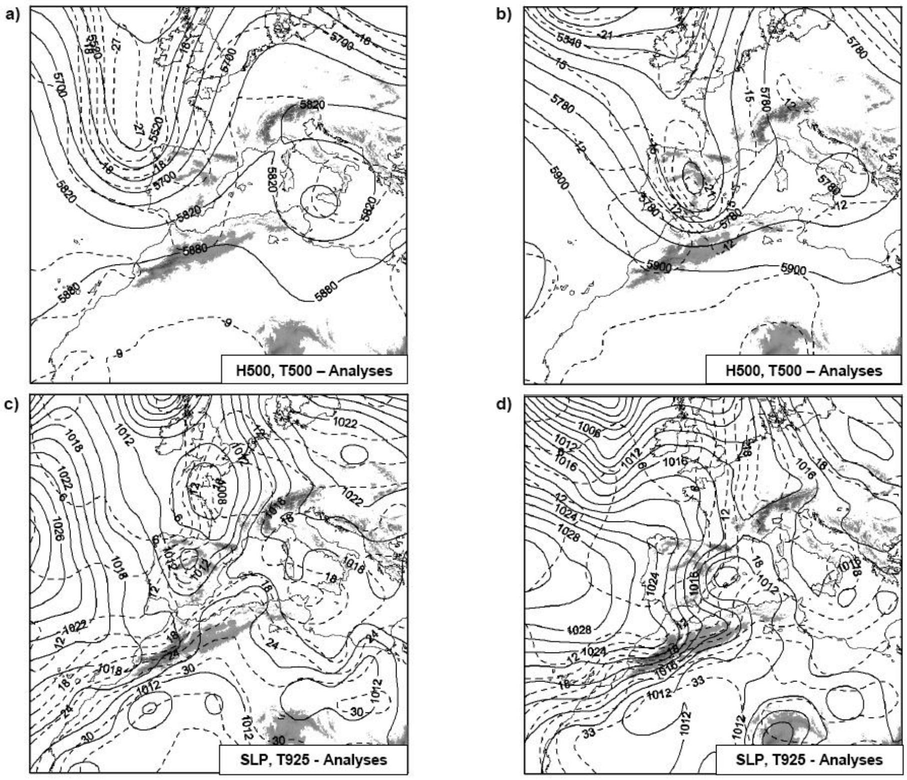

Figure 4.3. *NCEP (National Centers for Environmental Prediction) analyses maps. (top) Geopotential height at 500 hPa (continuous line, gpm) and temperature at 500 hPa (dashed line, ° C) at (a) 0000 UTC 9 June 2000 and (b) 0000 UTC 10 Jun 2000. (bottom) Sea level pressure (continuous line, hPa) and temperature at 925 hPa (dashed line, ° C) at (c) 0000 UTC 9 June 2000 and (d) 0000 UTC 10 Jun 2000. Main orographic systems are highlighted. Figure from Martín et al. (2007).*

This MEDEX cyclone is used to illustrate the potential of the presented methodology. The figure 4.4 shows the original initial state and four perturbed ensemble members for 9th June 2000 at 00 UTC. These initial states and the boundary conditions associated are introduced in the MM5 model to run a 54 h forecasts. The boundary conditions of the four perturbed ensemble members are perturbed too, using the same method described above. The figure 4.5 shows the MM5 54 h forecasts of the control and perturbed members for 11th June 2000 at 06 UTC.

The period of forecasting is 54 h to simplify the posterior verification process. That is because the rainfall data is available at 24 h intervals starting each day at 06 UTC.

A brief description of the ensemble member figures is done below.

- **Initial state:** (Fig. 4.4) The five ensemble members PV structures are different. The differences are provided by the displacement error that affects the spatial patterns and intensity error that affects the PV intensity distribution. The difference in intensity is bigger than the spatial ones. In spite of this it is obvious that all members represent the same PV structure and that this difference is due to reasonable uncertainties of the meteorological state.
- **54 h forecast:** (Fig. 4.5) The differences in the initial state and the boundary conditions are reflected on in the obtained forecasts. The rainfall patterns are clearly different, but contain the observed pattern. So, the ensemble captures the event. The sea level pressure and PV field at 300 hPa are different too. These differences are shown in the displacement of the fields, in the intensity differences and in the position of the PV center.

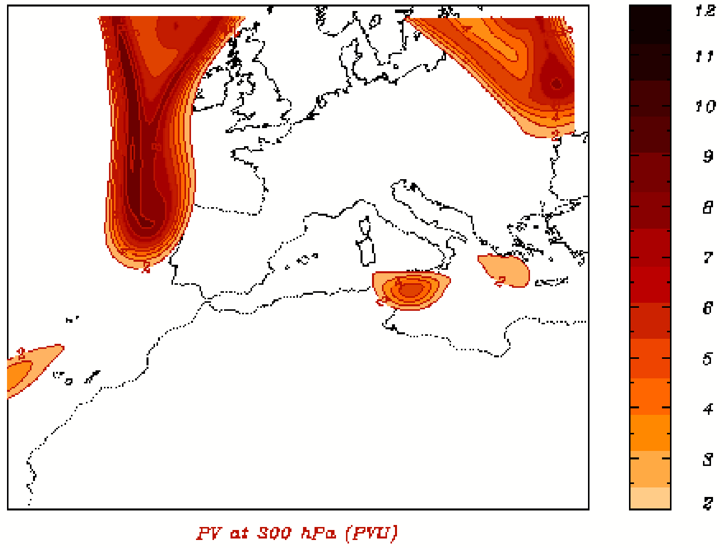

(a) *Control member*

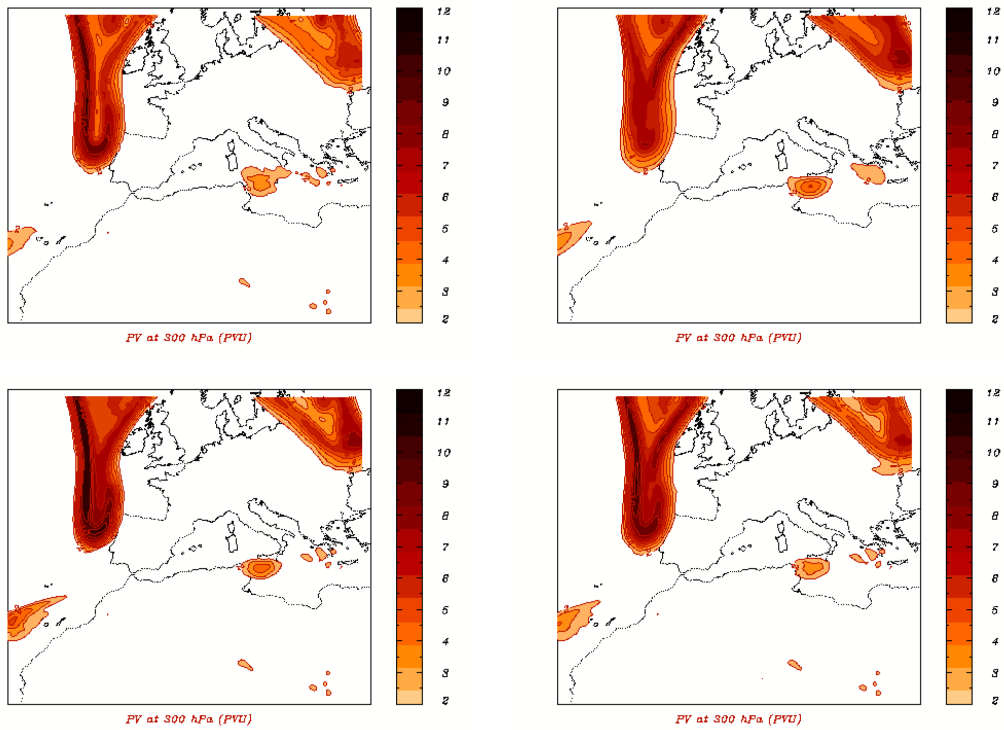

(b) *Perturbed members*

Figure 4.4. *9th June 2000 at 00 UTC. PV field at 300 hPa. Original initial state (control member) and four perturbed ensemble members*

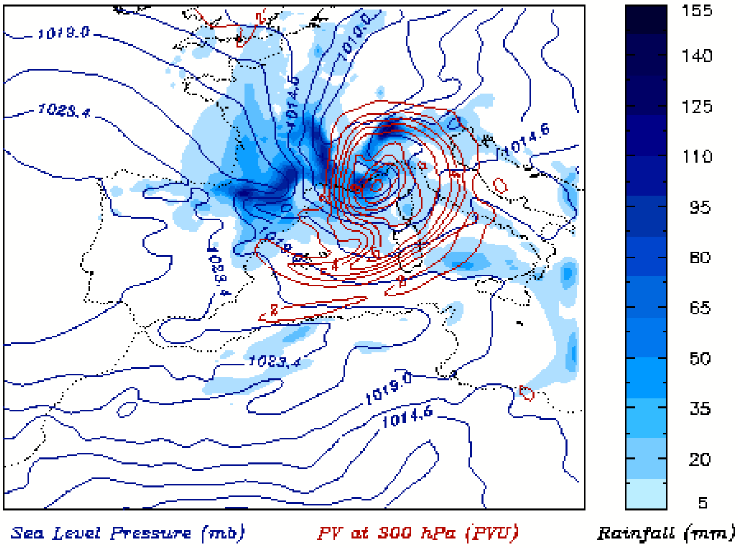

(a) *Control member*

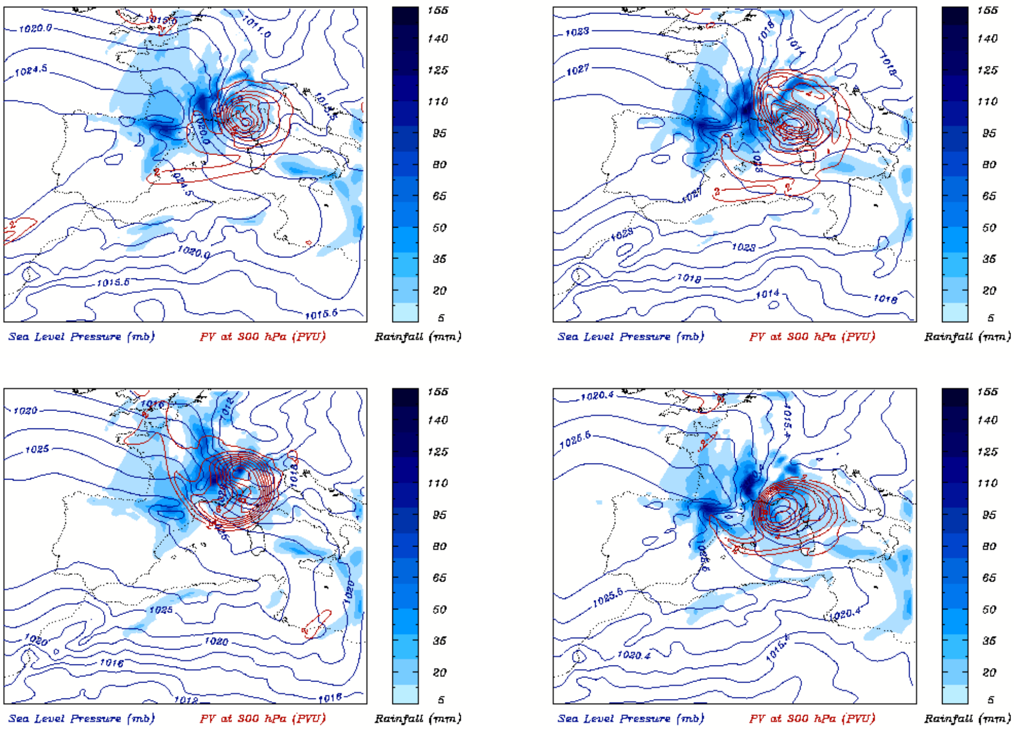

(b) *Perturbed members*

Figure 4.5. *MM5 54 h forecasts of 11th June 2000 at 06 UTC. Total rainfall (fill contour), sea level pressure (blue line) and PV field at 300 hPa (red line). Control member and four perturbed ensemble members*

Chapter 5

Conclusions and further work

The potential vorticity error climatology gathers up the real uncertainties in the PV field given by the ECMWF 24 h forecasts. This PVEC allows to perturb the ECMWF 24 h forecasts introducing reasonable errors that can account for the true state of the atmosphere. This uncertain initial state is the basic principle of the probabilistic forecasting. So, the PVEC can be used not only to improve the knowledge of the PV field but to design an ensemble system based on perturbed initial and boundary conditions.

The designed methodology appears to be a promising tool for building ensemble forecasts of extreme weather events such as high impact Mediterranean cyclones. The use of a single variable, PV, on which to define perturbations, combined with the PV inversion technique, keeps the method simple while ensures modifications of all the meteorological fields without compromising the mass-wind balance. The resulting forecasts are consistent with the real uncertainties of the PV field and produce precipitation fields of realistic variability.

In a further work, this method will be applied systematically, using 20 ensemble members, to all members of the MEDEX cyclones collection comprising 56 different simulation periods.

Another line of work consists of using the PV sensitivity areas calculated by the MM5 adjoint model instead of the zones with the most intense PV values and gradients previously explained.

An adjoint model is the transpose of the first-order linear approximation of the evolution of perturbations in the standard forward nonlinear simulations (Martín et al., 2007), and provides an excellent framework to determine the sensitivities of a particular forecast feature of interest, called response function (Fig.5.1). The adjoint model allows to evaluate the effect of any perturbation to one particular response function (Homar and Stensrud, 2004).

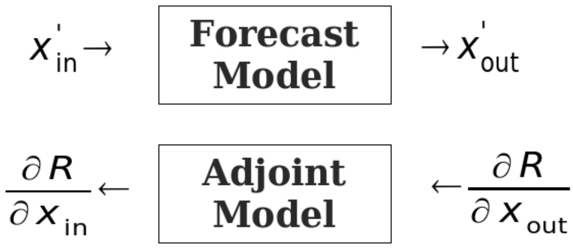

Figure 5.1. *Schematical view of an adjoint model. X_{in} are the initial meteorological fields, X_{out} are the simulated fields, and R is the response function of the adjoint model.*

As an example, the PV sensitivity areas of our study case are calculated by the MM5 adjoint under a response function given by the low-level vorticity predicted over the western Mediterranean region (Fig. 5.2). In this case perturbations of the PV field are introduced in closely following the spatial and intensity pattern of the sensitivity field.

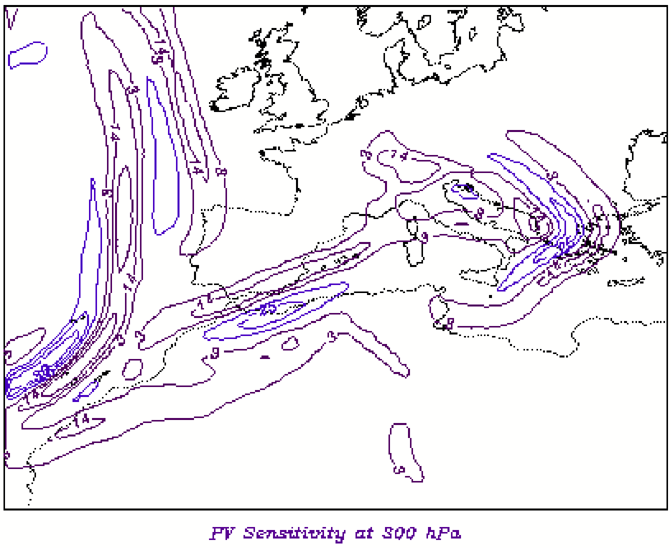

Figure 5.2. *MM5 adjoint PV sensitivity field at 300 hPa for the MEDEX cyclone of 9th June 2000 at 00 UTC. Positive values are in purple and negatives in lilac.*

Preliminary results seems to indicate that perturbing according to PV sensitivity patterns instead of randomly, produces higher spread and more realistic results, as figure 5.3 shows.

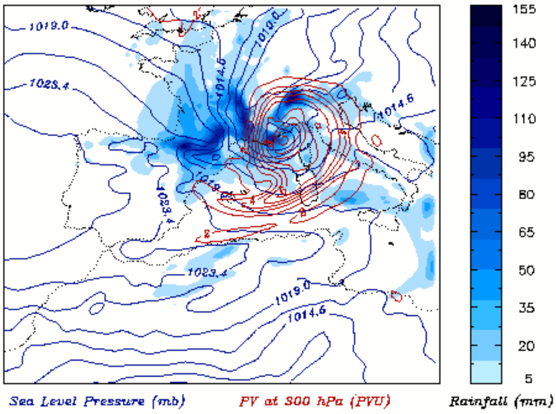

(a) *Control member*

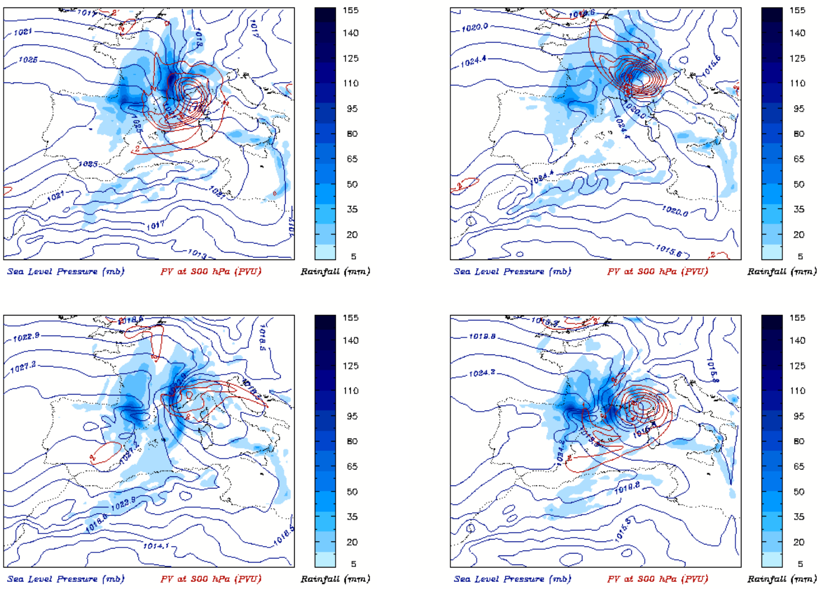

(b) *Perturbed members*

Figure 5.3. *MM5 54 h forecasts of 11th June 2000 at 06 UTC obtained using the MM5 adjoint PV sensitivity field. Total rainfall (fill contour), sea level pressure (blue line) and PV field at 300 hPa (red line). Control member and four perturbed ensemble members*

Bibliography

Bluestein, H. B., 1993: *Synoptic-dynamic meteorology in midlatitudes*, volume I and II. Oxford University Press.

Carlson, T. N., 1991: *Mid-Latitude Weather Systems*. Harper Collins Academic.

Charney, J. G., 1955: The use of primitive equation of motion in numerical prediction. *Tellus*, **7**, 22–26.

Davis, C. A. and K. A. Emanuel, 1991: Potential vorticity diagnostics of cyclogenesis. *Mon. Wea. Rev.*, **119**, 1928–1953.

Dudhia, J., 1993: A non-hydrostatic version of the Penn State/NCAR mesoscale model: Validation tests and simulation of an Atlantic cyclone and cold front. *Mon. Wea. Rev.*, **121**, 1493–1513.

Ertel, H., 1942: Ein neuer hydrodynamischer wirbelsatz. *Meteor. Z.*, **59**, 271–281.

Grell, G., J. Dudhia, and D. R. Stauffer, 1995: *A description of the fifth-generation of the Penn State/NCAR mesoscale model (MM5).* NCAR Tech. NCAR/TN-398+STR.

Holton, J. R., 1979: *An introduction to dynamic meteorology.* Academic Press.

Homar, V., C. Ramis, and S. Alonso, 2002: Numerical study of the October 2000 torrential precipitation event over eastern Spain: Analysis of the synoptic-scale stationarity. *Ann. Geophys.*, **20**, 2047–2066.

Homar, V. and D. J. Stensrud, 2004: Sensitivities of an intense Mediterranean cyclone: Analysis and validation. *Quart. J. Roy. Meteor. Soc.*, **130**, 2519–2540.

Hoskins, B. J., M. E. McIntyre, and A. W. Robertson, 1985: On the use and significance of isentropic potential vorticity maps. *Quart. J. Roy. Meteor. Soc.*, **111** (470), 877–946.

Jansà, A., A. Genovés, M. A. Picornell, J. Campins, R. Riosalido, and O. Carretero, 2001: Western Mediterranean cyclones and heavy rain. Part 2: Statistical approach. *Meteorol. Appl.*, **8**, 43–56.

Jordan II, M. R., 2005: *Using the superensemble method to improve eastern pacific tropical cyclone forecasting*. Ph.D. thesis, Florida State University.

Krishnamurti, T. N., C. M. Kishtawal, T. LaRow, D. Bachiochi, Z. Zhang, C. E. Williford, S. Gadgil, and S. Surendran, 1999: Improved weather and seasonal climate forecasts from multimodel superensemble. *Science*, **285**, 1548–1550.

Krishnamurti, T. N., C. M. Kishtawal, T. LaRow, D. Bachiochi, Z. Zhang, C. E. Williford, S. Gadgil, and S. Surendran, 2000a: Multi-model superensemble forecasts for weather seasonal climate. *J. Climate*, **13**, 4196–4216.

Krishnamurti, T. N., C. M. Kishtawal, D. W. Shin, and C. E. Williford, 2000b: Improving tropical precipitation forecasts from multianalysis superensemble. *J. Climate*, **13**, 4217–4227.

Krishnamurti, T. N., S. Surendran, D. W. Shin, R. Correa-Torres, T. S. V. Vijaya Kumar, C. E. Williford, C. Kummerow, R. F. Adler, J. Simpson, R. Kakar, W. Olson, and F. J. Turk, 2001: Real time Multianalysis/Multimodel Superensemble forecasts of precipitation using TRMM and SSM/I products. *Mon. Wea. Rev.*, **129**, 2861–2883.

Lorenz, E. N., 1963: Deterministic non-periodic flow. *J. Atmos. Sci.*, **20**, 130–141.

Martín, A., R. Romero, V. Homar, A. De Luque, S. Alonso, T. Rigo, and M. C. Llasat, 2007: Sensitivities of a flash flood event over Catalonia: a numerical analysis. *Mon. Wea. Rev.*, **135**, 651–669.

Romero, R., 2001: Sensitivity of a Heavy Rain Producing Western Mediterranean Cyclone to Embedded Potential Vorticity Anomalies. *Quart. J. Roy. Meteor. Soc.*, **127**, 2559–2597.

Romero, R., C. A. Doswel III, and R. Riosalido, 2001: Observations and fine-grid simulations of a convective outbreak in northeastern Spain: Importance of diurnal forcing and convective cool pools. *Mon. Wea. Rev.*, **129**, 2157–2182.

Romero, R., C. A. Doswell III, and C. Ramis, 2000: Mesoscale numerical study of two cases of long-lived quasistationary convective systems over eastern Spain. *Mon. Wea. Rev.*, **128**, 3731–3751.

Appendix A

Collection of MEDEX cyclones

A brief description of several MEDEX cyclones (http://medex.inm.uib.es).

	Date	**Priority**	**Country affected**	**Societal impacts**
01	11-12 Sep. 1996	Medium	Spain	Flood in Valencia region. Serious damages from winds in Bal. Isl. High risk for navigation
02	06-09 Oct. 1996	High	Italy (Sardinia; Emilia-Romagna), Spain (Balears)	Widespread floods, affect. 40000 people (Em. Rom.), minor floods (Sardinia)
03	14 Oct. 1996	Medium	Spain, Italy	Floods and damages in infrastructures. In IT (Calabria): floods, 6 casualties, buildings destroyed, interruption of terr. traffic, huge damages to agriculture, tourist and industrial activities

	Date	Priority	Country affected	Societal impacts
04	04-06 Nov. 1997	High	Portugal (S Alentejo), Spain, France (Med. coast, Cevennes, French Alps)	Floods (FR, SP,PO), casualties (FR, SP), material losses. 4 casualties (PO).
05	11-14 Nov. 1999	High	Italy (Sardinia), Spain, France	Serious floods, casualties (Sardinia). Severe flood, 30 casualties (FR), 1000 M Euros loss (FR)
06	10 Jun. 2000	High	Spain (Catalunya)	240 mm/6h, flood, 4 casualties in Catal., landslides, buildings and roads affected, very heavy material losses
07	21-26 Oct. 2000	High	Spain (Catal., SE of Aragon, N Valencian comm.)	Serious flash floods, 8 casualties in Catal. and other parts of Spain, landslides. Buildings and roads affected. Very important damages and losses.
08	02-05 Nov. 2001	Low	Spain (Murcia, Castellón, Málaga, Almería)	Important floods
09	09-13 Nov. 2001	High	Algeria, Spain (Balears), Croatia, Morocco	Disaster in Algiers: about 600 victims, thousands homeless. Floods also in Morocco. In Balears: 4 casualties, 220,000 trees uprooted, up to 60% sand removal in beaches, 100 M€ private damage, infrastructures damages, serious interruptions of traffic, electric power system and telephone.

	Date	**Priority**	**Country affected**	**Societal impacts**
10	14-16 Nov. 2001	High	Spain (Balears)	Damage was significant (added to the previous extreme impact), but the psychological impact (high perception of risk) was even more dramatic.
11	14-15 Dec. 2001	Medium	Spain (Catalonia)	Incommunicated roads, high roads and villages Damages in beaches
12	11 Apr. 2002	Low	Spain (North-eastern Catalonia: Empordà)	Damages in urban furniture Damages in beaches Local floods
13	06-08 May. 2002	Medium	Spain (Valencia, Balears)	Floods
14	12-15 Jul. 2002	Medium	Spain (Balears), Croatia	Big damages and 1 casualty (Croatia)
15	31 Jul. 2002 - 01 Aug. 2002	Medium	Spain (Eastern Catalonia)	Damages in urban furniture
16	08-10 Sep. 2002	High	France (Nimes-Marseille)	20-30 casualties, floods, serious interruption of railway and road traffic
17	12-13 Sep. 2002	Medium	Spain (Catalonia, Balears)	Important floods in both areas. 30 cars dragged out in Pollença
18	23-24 Sep. 2002	Medium	Spain (Central coast of Catalonia)	Local floods Damages in urban furniture
19	08-10 Oct. 2002	Medium	Spain (Central coast of Catalonia)	—

Acknowledgement

Support from PRECIOSO/CGL2005-03918/CLI project and PhD grant BES-2006-14044 (both from the Spanish *Ministerio de Educación y Ciencia*) is acknowledged.